Non-Iterative Object Detection Methods in Electrical Tomography for Robotic Applications

Stephan Mühlbacher-Karrer, Juliana P. Leitzke, Lisa-Marie Faller and Hubert Zangl

Institute of Smart Systems Technologies, Sensors and Actuators, Alpen-Adria-Universität Klagenfurt,
Universitätsstraße 65-67, A-9020 Klagenfurt
E-mail: stephan.muehlbacher-karrer@aau.at

***Abstract*—In this work we investigate the usability of the non-iterative monotonicity approach for Electrical Capacitance Tomography (ECT) based object detection. We introduce a new split up strategy for the Region of Interest (ROI) to improve the detection range and accuracy of the obtained detection image. The new split up strategy is compared with the unmodified algorithm to evaluate the improvements. Furthermore, we suggest a different approach to determine the threshold value for the exclusion test to avoid solving the minimization problem (and their implied forward problems) each time a new measurement is obtained to save computational costs speeding up the algorithm which is mandatory using the monotonicity approach for robotic applications with real time constrains.**

***Index Terms*—Capacitance, Tomography, Object detection, Non-Iterative methods, Monotonicity, ECT**

I. Introduction

For industrial and domestic robots, reliable object detection is a mandatory skill in a shared human-robot environment. Hence, a reliable robot perception with respect to object detection in the close surroundings of the robot is necessary. Many sensor technologies can be utilized to accomplish that and a huge research effort has gone into optical based perception and collision avoidance [1] in the past decades. However, optical based systems are prone to translucence, varying light conditions, mirroring effects, etc. In this case, complementary proximity sensors [2] based on, e.g., ECT may be used to overcome these perception gaps. Moreover, ECT comes with the advantage to provide object detection incorporating 2D position information (compared to proximity sensors providing 1D spatial information) of the approaching object. This can be combined with the ability to select subregions of the reconstructed ROI, where objects should be detected, e.g., for a 9 Degree of Freedom (DoF) serial manipulator to avoid self detection, i.e. detection of links that are part of the manipulator itself. Furthermore, the complete signal processing chain should satisfy the minimum speed requirement of a common robot control loop (1 ms).

In Fig. 1(a) it is shown how the ECT information can be used in a 9 DoF serial manipulator to avoid collision with a human while still performing its task. In such a situation the background material is the air, while the object to be reconstructed is the hand. In this case, the electrodes would not be placed around the complete ROI, but in a planar geometry on one side, as shown in Fig. 1(b).

The principle of ECT is based on the fact that each material has its own particular set of electrical properties. Therefore, it is possible to differentiate an object located in the ROI in contrast to the substance surrounding it, e.g. air, based on their permittivities. This permittivity distribution affects the capacitance, which can be measured between electrodes [3].

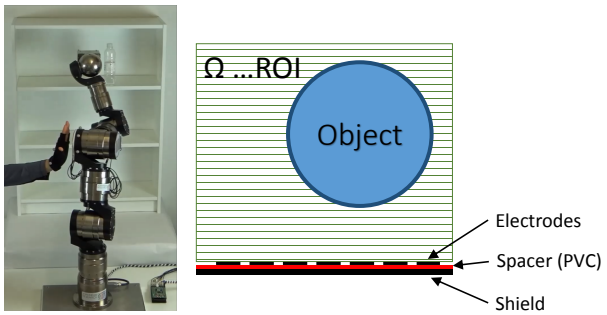

Fig. 1. Shared human-robot workspace (a) robot avoids collision with the human based on the ECT information while fulfilling its pick and place task (b) schematic setup of the ECT sensor front end for the object detection scenario.

A. Background

Many reconstruction algorithms have been developed for ECT. However, our focus is on methods that present low computational effort, which allows the reconstruction to be performed in an embedded system with microcontrollers. Non-iterative (or single step) algorithms offer the necessary complexity, such as fast Bayesian methods (BMMSE), a category where Optimal First Order Approximation (OFOA) and Optimal Second Order Approximation (OSOA) are included [4], methods that were already implemented for this application. Recently, object detection in ECT (with planar electrode geometry) based on hypothesis testing [5] has shown promising results with respect to speed and detection rate. However, the object detection performance is decreasing with increasing distance to the sensor front end. The currently used OFOA approach allows for introduction of non-linearities in the model by transformation, but otherwise it is still an approximation.

Another method that could be used for our application and that we aim to investigate is the non-iterative inversion method based on the monotonicity of the capacitance matrix, which offers a simple numerical implementation [6].

The non-iterative inversion algorithm based on the monotonicity of the resistance matrix for reconstructing a homogeneous inclusion placed in a homogeneous background material was first introduced in [7] for Electrical Resistance Tomography (ERT). This method can also be used in Electrical Impedance Tomography (EIT) [8], being further extended and an equivalent principle was applied for the capacitance matrix in ECT and for the second order moment associated to the conductivity in Magnetic Induction Tomography (MIT) based in induced eddy currents [9] [10] [11].

The computational effort of the monotonicity approach might be just slightly higher compared to OFOA due to the necessity to solve only very small eigenvalue problems (depends only on the number of electrodes), instead of a matrix vector multiplication, where the size of the matrix depends on the elements of the ROI and of the number of electrodes. Nevertheless, it should still be able to meet the requirements in the field of robotics and may provide for a better resolution.

B. Contribution

In this paper, we investigate the appropriateness of the monotonicity approach for object detection in ECT in the field of robotic applications for collision avoidance with respect to safety. In contrast to the classical monotonicity applications [7], the ROI Ω is not completely surrounded by electrodes in our application. Therefore, the split up of the ROI to solve the forward problem is adapted to be able to use the method for the detection of objects approaching the sensor front end, allowing it to be applied in robotic applications. The computational effort of the algorithm is further improved by avoiding to solve the minimization problem to find the threshold value for the exclusion test. Our adapted algorithm is evaluated against the original algorithm to demonstrate the performance of the proposed modifications.

The system description is presented in Section II, where the monotonicity approach is explained, as well as the object detection principle, the threshold value criterion and the discretization issue. The simulation setup is introduced in Section III, followed by the reconstructed detection results in Section IV and conclusion in Section V.

II. System Description

In ECT based object detection usually two steps are required. First, a reconstruction algorithm to obtain the spatial permittivity distribution (continuous values). Second, a detection algorithm to extract a detection image (binary values) from the reconstruction [5]. Another possibility to combine those two steps into a single one is the monotonicity approach from [7] introduced for ERT. This approach was further investigated for the classical ECT setup, e.g., mass flow in pipe with two-phase mixture (oil/gas), where the non-iterative monotonicity approach was combined with a Gauss Newton based schema to improve the accuracy of the reconstruction results [12].

In comparison to previous work, the monotonicity approach is adapted saving the cost of solving the forward problems in each step when a new measurement is obtained to find the optimal value for the threshold reducing the computational effort. In addition, due to the reduced number of electrodes and space constrains (electrodes are placed only on one side of the ROI, instead of around it), the split up pattern for the ROI is modified to use the monotonicity approach for robotic applications.

A. Monotonicity

The original monotonicity approach for ERT states that if the resistance matrix $R_{\rho_1} - R_{\rho_2}$ is a positive semidefinite matrix, then it satisfies the monotonicity property defined as

$$\rho_1(r) \geq \rho_2(r) \quad \forall r \in \Omega \Rightarrow R_{\rho_1} \geq R_{\rho_2} \tag{1}$$

where ρ is the resistivity and R_ρ is the corresponding resistance matrix [7].

In comparison to ECT, the obtained capacitance matrix $C_{\varepsilon_1} - C_{\varepsilon_2}$ (either from measurements or simulations) fulfills the same monotonicity properties. Consequently, the same algorithm as used for ERT can be applied for ECT and Eq. 1 can be rewritten for ECT to

$$\varepsilon_1(x) \geq \varepsilon_2(x) \quad \forall x \in \Omega \Rightarrow C_{\varepsilon_1} \geq C_{\varepsilon_2} \tag{2}$$

where ε is the permittivity and C_ε represents the corresponding capacitance matrix. Eq. 2 can be further reformulated to

$$C_{\varepsilon_1} - C_{\varepsilon_2} \geq 0 \tag{3}$$

which means that the matrix $C_{\varepsilon_1} - C_{\varepsilon_2}$ is positive semidefinite if $\varepsilon_1(x) \geq \varepsilon_2(x)$.

A capacitance matrix C can be obtained by the relation

$$C = QV^{-1} \tag{4}$$

where Q are the charges on the electrodes and V contains the linear independent voltage patterns applied on the electrodes.

The capacitance matrix is a symmetric matrix containing the capacitances from the single ended measurement mode (capacitance against distant ground) in the main diagonal and the differential measurement mode (capacitance between electrodes) in the side diagonals.

The original monotonicity method consists in separating a ROI Ω in N small non-overlapping parts, where Ω_k corresponds to the k_{th} element of Ω [7]. For $0 < \varepsilon_2 < \varepsilon_1 < \infty$, C_{Ω_k} is the matrix related to the permittivity

$$\varepsilon_k(x) = \begin{cases} \varepsilon_1 & \text{in } \Omega_k \\ \varepsilon_2 & \text{in } \Omega \setminus \Omega_k \end{cases} \quad (5)$$

where ε_2 is the permittivity of the environment, e.g., air, and ε_1 is the permittivity of the object (inclusion). Ω_{Obj} is defined as reconstruction of an object (inclusion) in Ω and is a union of some of these elements Ω_k.

B. Object Detection

The detection of an object is based on an exclusion test which can be defined in the following way

$$\Omega_k \in \Omega_{Obj} \Rightarrow C_{Obj} \geq C_{\Omega_k} |\ \varepsilon_k \leq \varepsilon_{Obj} \quad \varepsilon = 1\ elsewhere \quad (6)$$

This can be rewritten to

$$C_{Obj} \ngeq C_{\Omega_k} \Rightarrow \Omega_k \notin \Omega_{Obj} \quad (7)$$

If equation 7 is fulfilled, it is ensured that there is no object at the location of element Ω_k. Furthermore, if this holds for all elements in Ω it is ensured that there is no object present at all in Ω. However, it should be noted in case the equation does not hold, then we cannot exclude the presence of the object in this region.

C. Threshold value

A practical test criterion used in the presence of measurement noise is based on the determination of the sign index

$$s_k = \frac{\sum \lambda_{k,j}}{\sum |\lambda_{k,j}|} \quad (8)$$

where $\lambda_{k,j}$ is the j_{th} eigenvalue of the matrix $\check{C} - C_{\Omega_k}$ and it must be calculated in order to test if this matrix is positive semi-definite. $\check{C}$ is the measured capacitance matrix (obtained from the simulations).

Considering the presence of noise in the measurement and that we are reconstructing the exterior dimensions of an object (inclusion), the value of the sign index s_k, defined in Eq. 8, must follow

$$s_k < s_{th} \quad (9)$$

when there is no object (inclusion) present at element Ω_k. In other words, once Eq. 9 is satisfied, then no object is present at location of element Ω_k. The threshold value s_{th} is usually determined by solving a 1d minimization problem of a monotonic function which implies to solve the forward problem until the optimal value is found which can be computationally intensive as it involves the solutions of forward problems. In [11] it was further suggested to use a non-linear transformation $\hat{s}_k = \frac{1}{1-s_k}$ to avoid to determine s_{th} and directly obtain the detection image. However, to further process the detection image for, e.g., robotic applications in both cases (using either s_k or $\hat{s}_k$) a threshold value is required to decide if an object is present or not at a certain location. Therefore, we propose a strategy to avoid solving any forward problem again each time a new measurement is obtained

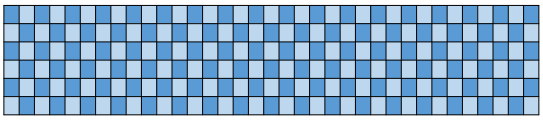

Fig. 2. Common split up pattern of the ROI as used in classical ERT applications [7].

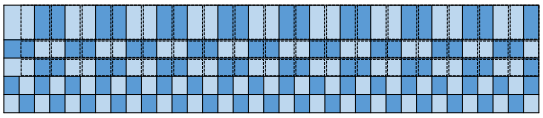

Fig. 3. Split up pattern of the ROI considering increasing objects with increasing distance to the sensor front end to solve the forward problem.

to reduce the computational effort of the algorithm. In our strategy we take the measurement noise instead of the measurement data and determine s_k. From this point we empirically determine the threshold value s_{th} in a way that the probability to detect an object only in presence of noise is negligible by means of Monte Carlo simulations. It should be noted that in a real setup the measurement noise of the measurement hardware has to be taken to determine the threshold value s_{th}.

D. Discretization Issue

The discretization of Ω is crucial due to the spatial constraints of the placement of the electrodes, which are located only on one side of Ω. Considering C_{empty} the capacitance matrix with no object present, in case the size of Ω_k is very small then $(C_{\Omega_k} - C_{empty}) \approx 0$ which can be insufficient to change the sign of the eigenvalues in the presence of measurement noise leading to the problem that we cannot exclude the element even if there is no object at a certain element. Consequently, we suggest to increase the size of the elements Ω_k with increasing distance to the electrodes to overcome this problem. In Fig. 3 the new split up strategy for Ω is shown in comparison the original strategy presented in Fig. 2. Furthermore, in comparison to [13], where the grouping of elements is suggested to be done over the entire ROI in this approach the size of the elements is increased only in areas which are further away from the electrodes.

III. Simulation Setup

In order to perform the necessary voltage and charge measurements to determine the matrices $\check{C}$ and C_{Ω_k}, required for the computation of the index s_k, simulations were made for different configurations using Finite Element Method (FEM), where the charge on each electrode was calculated as

$$Q = \oint_A D \cdot dA \quad (10)$$

where A is the area of the electrode surface and D the displacement field. With the calculated charge we can

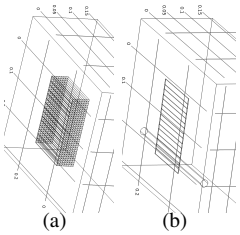

Fig. 4. (a) 3D FEM simulation model to solve the forward problem. (b) 3D FEM simulation model to obtain measurement data from the simulation where an object approaches the sensor front end.

then easily obtain the capacitance using the relation in equation 4.

The forward model (see Fig. 4(a)) is solved using a sensor front end comprising seven electrodes on a planar surface, each electrode has dimensions $12\,\mathrm{mm} \times 152\,\mathrm{mm} \times 0.035\,\mathrm{mm}$ (width $\times$ depth $\times$ height) and the adjacent distance of $15\,\mathrm{mm}$ is present between the electrodes. The size of Ω is set to $x = 201\,\mathrm{mm}$ and $y = 50\,\mathrm{mm}$, where x is the length of the planar surface and y is the perpendicular distance.

For the original and the new proposed monotonicity split up pattern, Ω is separated into $N = 245$ and $N = 206$ elements according to Fig. 2 and 3, respectively. In addition, the reduced number of elements in Ω saves the computational costs to solve the forward problem.

To generate the measurement data, the simulation model in Fig. 4(b) is used, where a different mesh is applied in order to avoid inverse crime, which could happen if the same mesh that was used to solve the forward problem and to obtain the data. Furthermore, to eliminate errors introduced by remeshing due to the repositioning of the object, the model is solved twice. Considering air as the background material with permittivity $\varepsilon = 1$, the simulation model is initially solved for an object with permittivity $\varepsilon = 1$ and then, on a different simulation, for an object of same geometry and position, but with the desired dedicated permittivity value of the object, e.g., $\varepsilon = 3.4$.

IV. Detection Results

The obtained threshold value used for all experimental results is $s_{th} = 0.97$. The reconstructed detection image of an object located in the ROI was retrieved after performing the proposed non-iterative monotonicity approach to the measurements obtained from the simulations, which consisted of a rod like inclusion with known permittivity placed in front of the electrodes at different locations. In addition, two distinct discretization patterns were used for the reconstruction, being compared for these different object locations.

In Fig. 5 the simulation results for an object far away from the electrodes are presented, comparing both the original and proposed split up strategy. In the detection image of the original split up strategy (see Fig. 5(a)) the excluded area is smaller in comparison to the new proposed strategy. The detection image of the new split up strategy (see Fig. 5(b)) shows a good match of the excluded area and the true position of the object. Furthermore, the distribution of the sign index s_k becomes sharper in the region of the position of the object, which results in an improvement of the excluded area in the corresponding detection image.

The simulation results for an object close to the electrodes using both the original and proposed split up strategy are presented in Fig. 6. Comparing Fig. 5(a) and Fig. 6(a), with decreasing distance inside the ROI the exclusion results becomes worse. The result for the equal pattern size for the split up of the ROI (see Fig. 6(a)) shows that the objects cannot be excluded at a distance $y \geq 30\,\mathrm{mm}$, which would make the original discretization method of the ROI unusable for robotic applications, where also subregions of ROI should be selectable for the object detection, e.g., only objects in the subregion $x > 200\,\mathrm{mm}$. In comparison, applying the new proposed split up strategy (see Fig. 6(b)), the region where the object can be excluded increases significantly, implying that the region where an object is possibly present is being restricted, which indicates a better result. Thus, a selection of subregions of ROI is realizable compared to the original approach, where an object close to the electrodes cannot be excluded along the entire x direction.

The proposed split up pattern enables to use the monotonicity approach for robotic applications, where the spatial placement of the electrodes is constrained to a planar geometry. In addition, due to the improvements in the exclusion tests, the selection of subregions in the ROI is made possible to avoid self detection in certain situations.

V. Conclusion

The presented simulation results have shown that the adapted split up patterns for the ROI improve significantly the accuracy of the results in comparison to the traditional ROI patterns, what makes the monotonicity approach applicable for ECT based object detection for applications with a reduced number of electrodes and spatial constrained placement of them, such as in robotics. The results further show that the exclusion test is sufficient to obtain a non-iterative object detection image, where the selection of subregions in a ROI is possible.

A new approach to find the threshold value for the test criterion was presented to reduce the computational cost for monotonicity based object detection using ECT. Furthermore, the different split up strategy reduces the number of elements, reducing the amount of forward problems which have to be solved for each obtained measurement data, further decreasing the required computational effort.

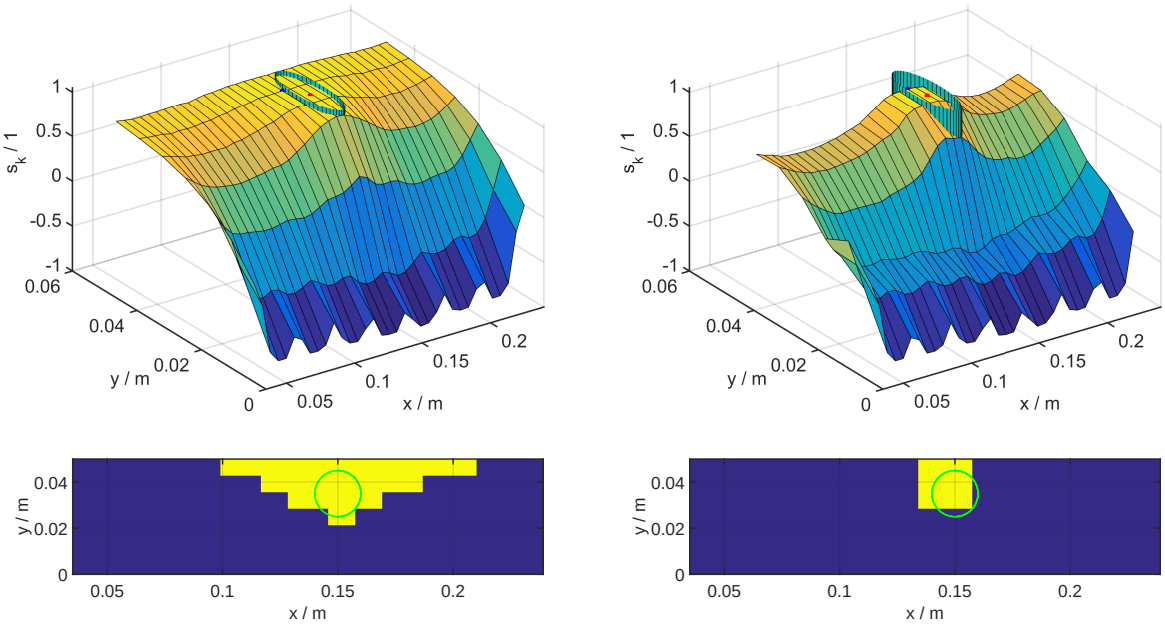

Fig. 5. Monotonicity approach for an object further away from the electrodes using a) original split up pattern and b) proposed split up strategy. Distribution of the sign index s_k while an object (blue cylinder) is placed inside the ROI. The red dot depicts the center of the cylinder and the blue dot depicts the maximum value of s_k. In each corresponding detection image the object is depicted by a green circle. The blue color shows the area where no object is present and yellow depicts the area where an object cannot be excluded.

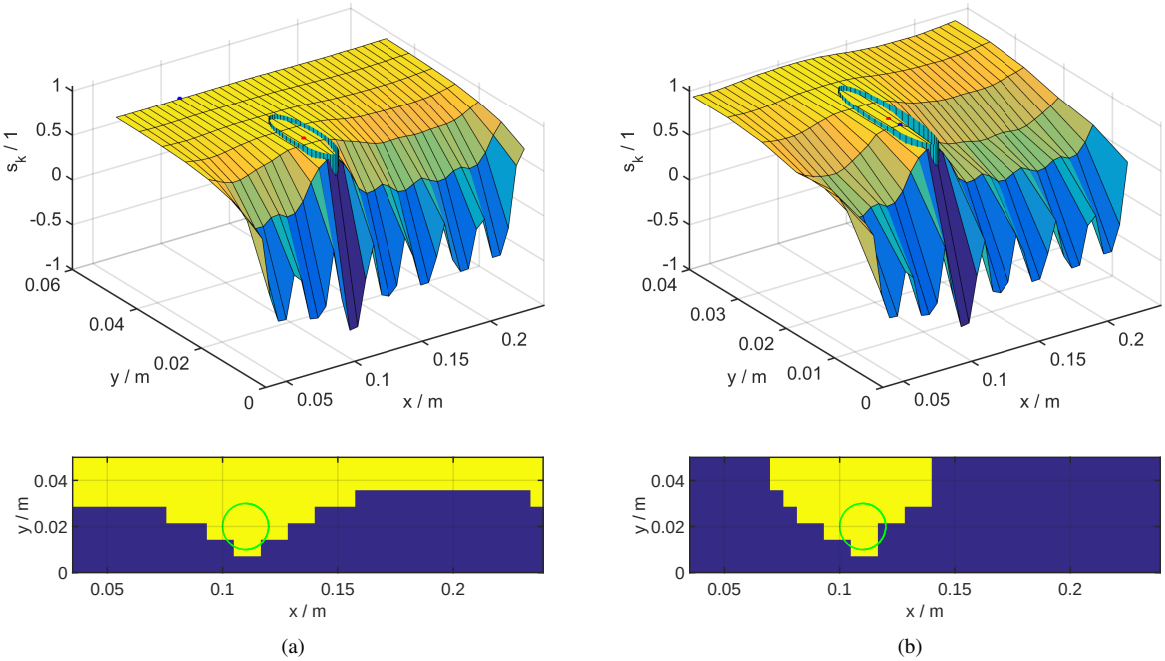

Fig. 6. Monotonicity approach for an object close to the electrodes using a) original split up pattern and b) proposed split up strategy. Distribution of the sign index s_k while an object (blue cylinder) is placed inside the ROI. The red dot depicts the center of the cylinder and the blue dot depicts the maximum value of s_k. In each corresponding detection image the object is depicted by a green circle. The blue color shows the area where no object is present and yellow depicts the area where an object cannot be excluded.

REFERENCES

[1] F. Flacco, T. Kröger, A. De Luca, and O. Khatib, "A depth space approach to human-robot collision avoidance," in *IEEE International Conference on Robotics and Automation (ICRA)*. IEEE, 2012, pp. 338–345.

[2] T. Schlegl, T. Kroger, A. Gaschler, O. Khatib, and H. Zangl, "Virtual whiskers - highly responsive robot collision avoidance," in *IEEE/RSJ International Conference on Intelligent Robots and Systems (IROS)*, Nov 2013, pp. 5373–5379.

[3] W. Yang and L. Peng, "Image reconstruction algorithms for

electrical capacitance tomography," *Meas. Sci. Technol.*, vol. 14, no. 1, pp. R1–R13, January 2003.

[4] H. Zangl, D. Watzenig, G. Steiner, A. Fuchs, and H. Wegleiter, "Non-iterative reconstruction for electrical tomography using optimal first and second order approximations," in *Proceedings of the 5th World Congress on Industrial Process Tomography*, Bergen, Norway, September 3-6, 2007, pp. 216–223.

[5] S. Mühlbacher-Karrer and H. Zangl, "Object detection based on electrical capacitance tomography," in *IEEE Sensors Applications Symposium*, 2015.

[6] A. Maffucci, A. Vento, S. Ventre, and A. Tamburrino, "A novel technique for evaluating the effective permittivity of inhomogeneous interconnects based on the monotonicity property," *IEEE Transactions on Components, Packaging and Manufacturing Technology*, vol. 6, no. 9, pp. 1417–1427, 2016.

[7] A. Tamburrino and G. Rubinacci, "A new non-iterative inversion method for electrical resistance tomography," *Inverse Problems*, vol. 18, no. 6, p. 1809, 2002.

[8] B. Harrach and M. Ullrich, "Monotonicity-based shape reconstruction in electrical impedance tomography," *SIAM Journal on Mathematical Analysis*, vol. 45, no. 6, pp. 3382–3403, 2013.

[9] M. Soleimani, "Computational aspects of low frequency electrical and electromagnetic tomography: a review study," *Int. Journal Numerical Analysis and Modeling*, vol. 5, no. 3, pp. 407–440, 2008.

[10] A. Tamburrino, G. Rubinacci, M. Soleimani, and W. Lionheart, "A noniterative inversion method for electrical resistance, capacitance and inductance tomography for two phase materials," in *Proc. 3rd World Congress on Industrial Process Tomography, Canada*. Citeseer, 2003, pp. 233–238.

[11] A. Tamburrino and G. Rubinacci, "Fast methods for quantitative eddy-current tomography of conductive materials," *IEEE transactions on magnetics*, vol. 42, no. 8, pp. 2017–2028, 2006.

[12] C. Wallinger, D. Watzenig, G. Steiner, and B. Brandstätter, "Adaptive monotonicity method for permittivity imaging," *COMPEL-The international journal for computation and mathematics in electrical and electronic engineering*, vol. 28, no. 4, pp. 892–906, 2009.

[13] G. Rubinacci, A. Tamburrino, and S. Ventre, "Regularization and numerical optimization of a fast eddy current imaging method," *IEEE Transactions on Magnetics*, vol. 42, no. 4, pp. 1179–1182, April 2006.